

01 Jul 2006

# Millimeter-Wave Detection of Localized Anomalies in the Space Shuttle External Fuel Tank Insulating Foam

Sergey Kharkovsky
*Missouri University of Science and Technology*

R. Zoughi
*Missouri University of Science and Technology*, zoughi@mst.edu

J. T. Case

Mohamed A. Abou-Khousa

*et. al. For a complete list of authors, see https://scholarsmine.mst.edu/ele_comeng_facwork/1727*



## Recommended Citation

S. Kharkovsky et al., "Millimeter-Wave Detection of Localized Anomalies in the Space Shuttle External Fuel Tank Insulating Foam," *IEEE Transactions on Instrumentation and Measurement*, vol. 55, no. 4, pp. 1250-1257, Institute of Electrical and Electronics Engineers (IEEE), Jul 2006.
The definitive version is available at https://doi.org/10.1109/TIM.2006.876543

# Millimeter-Wave Detection of Localized Anomalies in the Space Shuttle External Fuel Tank Insulating Foam

Sergey Kharkovsky, *Senior Member, IEEE*, Joseph T. Case, *Student Member, IEEE*, Mohamed A. Abou-Khousa, *Student Member, IEEE*, Reza Zoughi, *Fellow, IEEE*, and Frank L. Hepburn

***Abstract*—The Space Shuttle Columbia's catastrophic accident emphasizes the growing need for developing and applying effective, robust, and life-cycle-oriented nondestructive testing (NDT) methods for inspecting the shuttle external fuel tank spray on foam insulation (SOFI). Millimeter-wave NDT techniques were one of the methods chosen for evaluating their potential for inspecting these structures. Several panels with embedded anomalies (mainly voids) were produced and tested for this purpose. Near-field and far-field millimeter-wave NDT methods were used for producing images of the anomalies in these panels. This paper presents the results of an investigation for the purpose of detecting localized anomalies in several SOFI panels. To this end, continuous-wave reflectometers at single frequencies of 33.5, 70, or 100 GHz representing a relatively wide range of millimeter-wave spectrum [Ka-band (26.5–40 GHz) to W-band (75–110 GHz)] and utilizing different types of radiators were employed. The resulting raw images revealed a significant amount of information about the interior of these panels. However, using simple image processing techniques, the results were improved in particular as it relates to detecting the smaller anomalies. This paper presents the results of this investigation and a discussion of these results.**

***Index Terms*—Insulating foam, millimeter waves, nondestructive testing (NDT), Space Shuttle, spray on foam insulation (SOFI).**

## I. Introduction

THE SPACE Shuttle Columbia's catastrophic failure has been attributed to a piece of external tank spray on foam insulation (SOFI) striking the leading edge of the left wing of the orbiter causing significant damage to some of the protecting heat tiles [1]. There is an urgent need for an advanced nondestructive testing (NDT) technique capable of inspecting the external tank SOFI during and subsequent to the application of the foam and prior to a launch. Such a comprehensive inspection technique enables NASA to perform "life-cycle" inspection on the external tank and its supporting hardware. Consequently, NASA Marshall Space Flight Center initiated an investigation into several potentially viable NDT techniques for this purpose [2]–[7]. One such method involves the use of millimeter-wave NDT techniques to achieve these goals [3], [5]–[7]. The results of these investigations, on panels that provided for different and important geometries related to the complex structural properties of the external tank, have clearly pointed to the effective potential utility of millimeter-wave NDT techniques for testing the Space Shuttle external tank SOFI [6]. However, to better understand the capabilities and limitations associated with these techniques, there is a need for a systematic investigation into evaluating the capabilities of these techniques for detecting localized anomalies (i.e., voids) of different sizes and at different depths with the SOFI.

This paper presents the results of an investigation for the purpose of detecting localized anomalies in several SOFI panels. To this end, millimeter-wave continuous wave (CW) reflectometers at single frequencies of 33.5, 70, or 100 GHz representing a relatively wide range of millimeter-wave spectrum [Ka-band (26.5–40 GHz) to W-band (75–110 GHz)] and utilizing different types of radiators were employed in conjunction with several specially manufactured SOFI panels. Finally, the results of applying a simple image processing algorithm on the obtained images, for improving the measurement results, are also provided.

## II. Sample Specification and Measurement Approach

Millimeter-wave NDT methods have been used in a wide range of applications [8]. Signals at millimeter-wave frequencies are attractive for inspecting low-loss dielectric materials because they can penetrate inside of these materials with relative ease. Moreover, the relatively small wavelengths associated with these signals render high-spatial-resolution images of the interior of various complex, thick, and layered composite structures [8], [9]. The Space Shuttle's external fuel tank SOFI is in the family of low-permittivity and low-loss dielectric materials. The relative dielectric properties of the SOFI was measured at X-band, using a completely filled rectangular waveguide approach, to be $\varepsilon_r = 1.05 - j0.003$ [2]. This is expected because the foam is primarily composed of small air bubbles contained in a low-permittivity and low-loss polymer. In addition, the SOFI is a homogeneous material at millimeter-wave frequencies due to the small size of the air bubbles compared with the operating wavelengths (i.e., several orders of magnitude smaller). Two different sets of SOFI samples were produced for this investigation in which cylindrical voids with different diameters and heights were milled (i.e., drilled out).

Manuscript received June 15, 2005; revised March 22, 2006. This work was supported by the NASA Marshall Space Flight Center through a Cooperative Agreement.

S. Kharkovsky, J. T. Case, M. A. Abou-Khousa, and R. Zoughi are with the Applied Microwave Nondestructive Testing Laboratory, Department of Electrical and Computer Engineering, University of Missouri–Rolla, Rolla, MO 65409 USA.

F. L. Hepburn is with NASA Marshall Space Flight Center, Marshall Space Flight Center, AL 35812 USA.

Digital Object Identifier 10.1109/TIM.2006.876543

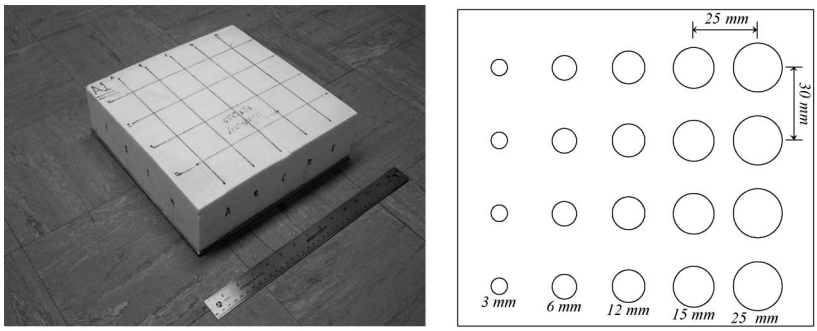


Fig. 1. SOFI panel (75 mm thick) with 20 embedded voids. (a) Picture. (b) Top view schematic.

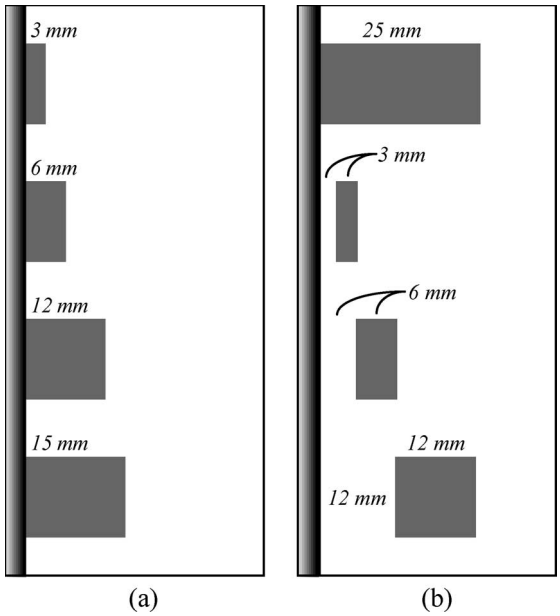


Fig. 2. Side view schematic of the 75-mm-thick SOFI. (a) Panel #1. (b) Panel #2.

### A. Sample Set #1

The first set of samples consisted of two SOFI panels (300 × 300 mm wide and 75 mm thick), each adhered to an aluminum substrate. A set of 20 cylindrical voids were milled in (drilled out) each panel. Fig. 1(a) shows the picture of one of these panels, whereas Fig. 1(b) shows the schematic of the relative locations of the 20 voids and their diameters, which ranged between 3 and 25 mm. The height of these voids and their locations above the aluminum substrate (i.e., location within the panel thickness) varied for each panel as shown in Fig. 2(a) and (b) (designated as panels #1 and #2), respectively. The combination of these panels provided for a geometrically diverse number of embedded voids. It must be noted that although these embedded anomalies mostly took the shape of cylindrical cavities/voids, the ones with relatively small heights actually simulate unbonds and delaminations in SOFI.

### B. Sample Set #2

The second sample set consisted of four SOFI slabs (550 × 240 mm wide and 70 mm thick). In one of these slabs, five cylindrical voids (i.e., flat-bottom holes) with a diameter of 25 mm and with heights of very close to 25, 18, 12, 6, and 3 mm were milled. The spacing between the centers of any two voids was about 95 mm. Fig. 3 shows the side and top schematic views of this panel (Fig. 3(a) shows the slab on top of an aluminum substrate). Another slab was similarly manufactured except that the void diameters were 6 mm. The other two slabs did not have any voids in them. Consequently, each of the slabs with the five flat-bottom holes could be used in conjunction with those devoid of holes to produce testing sample panels in which the height of the voids above an aluminum substrate could be varied using different combinations of the three SOFI slabs. In this way, localization of the voids at different depth from an aluminum substrate could be accommodated. The schematics of the possible combinations that were subsequently used in this investigation are shown in Fig. 4.

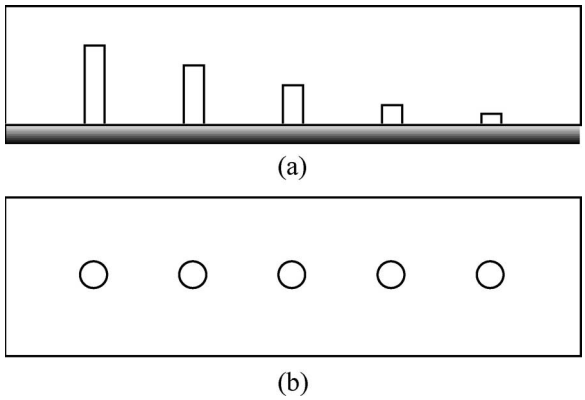


Fig. 3. (a) Side view and (b) top view schematic of the 70-mm-thick SOFI single-slab panel.

### C. Experimental Setup

In this investigation, several laboratory-designed millimeter-wave CW reflectometers were used for producing images of these panels at single frequencies of 33.5, 70, or 100 GHz. Some of these experiments involved the use of radiators such as small horn antennas with the panels primarily placed in their near-field regions, whereas others consisted of inspecting the panels in the far field of a focused lens antenna. When a panel is placed in the near-field region of a horn antenna, the resulting

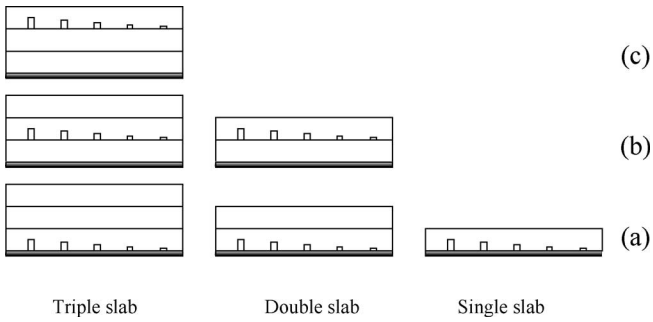


Fig. 4. Side view schematic of SOFI panels with voids located at different depths. (a) At substrate. (b) 70 mm from substrate. (c) 140 mm from substrate.

image possesses a relatively high spatial resolution. This is due to the fact that when operating in the near-field region of a probe/antenna, spatial resolution is primarily a function of the probe size [8]. Focusing lens antennas can produce much smaller footprints (e.g., narrow beamwidths) at their designed focal length (i.e., far field) [10]. The footprint associated with the two lens antennas used in this investigation was 12 and 6 mm at the focal length of 254 mm at the operating frequency of 100 GHz.

The SOFI panels were placed on two-dimensional (2-D) automated scanning tables, whereas the reflectometers were held at a fixed position above the panels. In this way, 2-D scans/images of the panels were produced at different frequencies and standoff distances (e.g., the distance between the radiator and the surface of a panel). A dc voltage, proportional to changes of the phase and magnitude of the reflected signal from the panel under test, was then measured and recorded in a matrix corresponding to the scanning area. Subsequently, the measured voltages in this matrix were normalized (with respect to the highest voltage value), and a grayscale image of the panel was produced.

## III. Results

Fig. 5(a)–(c) shows the images of SOFI panel #1 obtained at frequencies of 33.5 GHz (Ka-band), 70 GHz (V-band), and 100 GHz (W-band) using the near-field approach with a small horn antenna, whereas Fig. 5(d) shows the image of this panel at 100 GHz using the lens antenna with the 6-mm-diameter footprint. Dimensions in these images as well as all other images in this paper are in millimeters. Fig. 5(a) shows the Ka-band images of the voids, which are manifested by circular indications. The indication at the bottom right-hand corner of the image is that of a void with a diameter of 25 mm and a height of 15 mm placed on the aluminum substrate, whereas the indication at the top right-hand corner is due to a similar void but with a height of 3 mm. As expected, the indication of the former void is stronger than the latter due to the difference between their respective heights. On the other hand, it was unexpected to see that the indications of voids located in the middle of the panel (second and third rows from the top) are stronger than indications of larger voids. The reason for this will be explained later. From Fig. 5(a), it is clear that at least 17 of the voids are readily detected. The three voids that are not readily detected (the three voids from the top in the left-hand column) correspond to the smallest voids in this panel all with diameters of 3 mm and heights of 3, 6, and 12 mm, respectively. However, some of these voids were detected at higher frequencies. For instance, the smallest void with diameter of 3 mm and height of 3 mm can be seen in the top left corner of the 100-GHz image of the panel, as shown in Fig. 5(d). These results also illustrate the positive effect of the higher spatial resolution at 100 GHz. Moreover, higher frequency reflectometers are capable of detecting voids in the SOFI and other anomalies such as nonuniformities in the adhesive layer between SOFI and the substrate [Fig. 5(b)–(d)]. The 100-GHz image [Fig. 5(c)] using a small horn antenna provides more details about the adhesive layer than the 33.5- and 70-GHz images [Fig. 5(a) and (b)], as expected. In this case, small voids in this panel were not detected either, because of the nonuniformities of the adhesive layer that masked these small voids. Fig. 5(d) shows the image of the panel at 100 GHz using the 6-mm-diameter footprint lens antenna. The results give void dimensions that are close to their actual dimensions. The curvy features in these images [Fig. 5(b)–(d)] are associated with the nonuniformities of the adhesive layer. The presence of this nonuniformity is also the reason why some of the voids whose locations coincided with it had stronger indications in Fig. 5(a) (i.e., constructive interference).

SOFI panel #2 was scanned using small horn antennas at Ka-band and V-band, as shown in Fig. 6(a) and (b). In both images, the circular indications of the voids are clearly evident, similar to panel #1. The indication at the top right-hand corner of the image is that of a void with a diameter of 25 mm and a height of 25 mm placed right above the aluminum substrate, whereas the indication at the bottom right-hand corner is that of the void with a diameter of 25 mm and a height of 12 mm located 13 mm above the substrate [see Fig. 2(b)]. As expected, the former indication is much stronger than the latter due to the difference between volumes of the voids. The three voids that are not visible in Fig. 6(a) (the three voids from the bottom in the left-hand column) correspond to the smallest voids with diameters of 3 mm and heights of 12, 6, and 3 mm, respectively. These three voids were placed 12, 6, and 3 mm above the aluminum substrate, respectively. It should be noted that these voids could be masked by the nonuniformity associated with the adhesive layer, which can be seen near their locations in the V-band image [a dark patch in Fig. 6(b)]. Comparison between the 70-GHz images of panels #1 and #2 [Figs. 5(b) and 6(b)] shows that the application of the adhesive in panel #2 was more uniform than that in panel #1. Nevertheless, the image of panel #2 indicates nonuniformities associated with the adhesive layer in the top and bottom right corners of the panel as well as in the area of the two left-hand columns in the middle of the panel. Subsequently, the SOFI in panel #2 was cut away at the base from the substrate and placed on a different aluminum substrate without using any adhesive. Fig. 7 shows the image of this panel at 70 GHz, indicating the absence of the adhesive layer and the nonuniformity that was associated with it before. It is very likely that the smallest voids in this panel were not detected because their heights were significantly reduced as a result of cutting the SOFI.

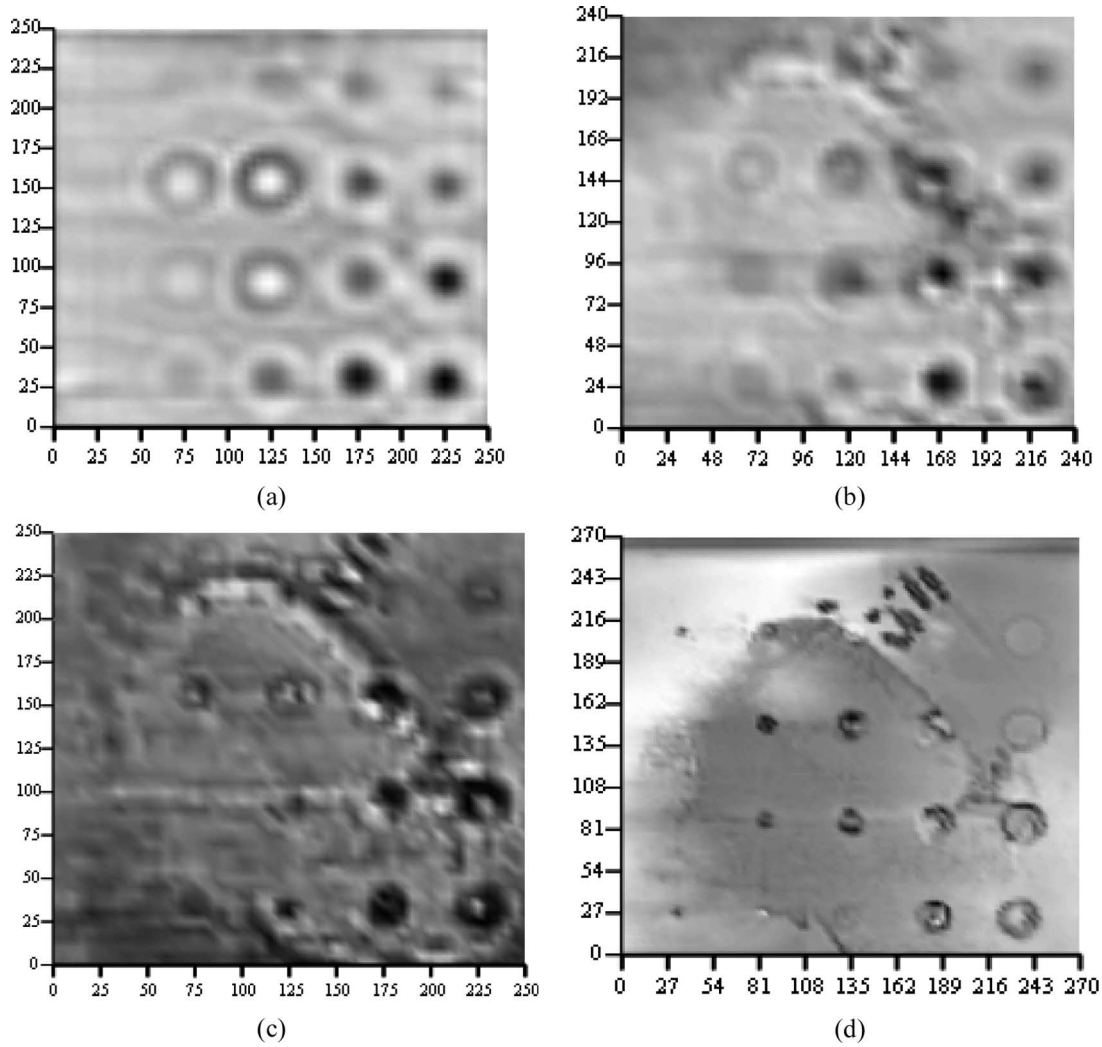


Fig. 5. Millimeter-wave image of panel #1. (a) 33.5 GHz using a horn antenna. (b) 70 GHz using a horn antenna. (c) 100 GHz using a horn antenna. (d) 100 GHz using the 6-mm-diameter footprint lens antenna.

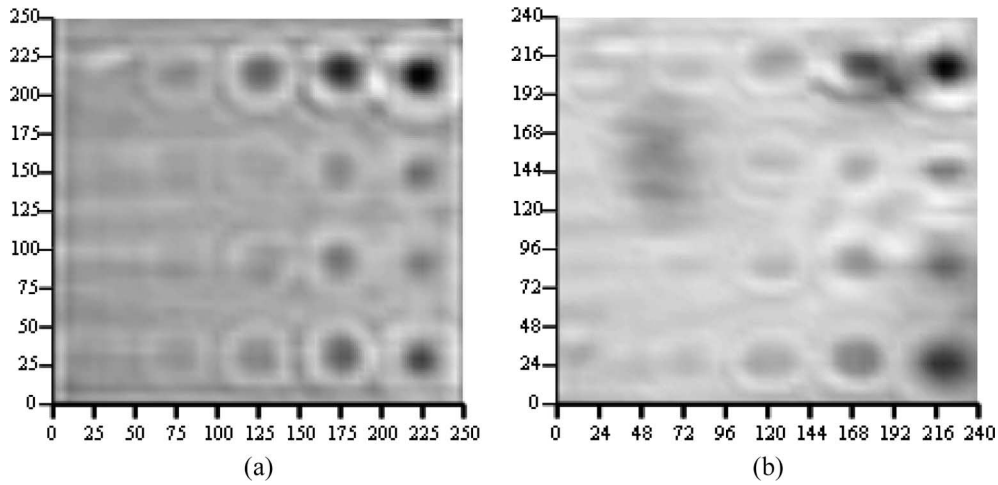


Fig. 6. Millimeter-wave image of SOFI panel #2 using a small horn antenna at (a) 33.5 GHz and (b) 70 GHz.

Figs. 5–7 are raw images, and no signal/image processing was applied to them. This is significant because they show the effectiveness of these millimeter-wave NDT methods for producing rapid and informative images of the interior of SOFI. The results shown in Figs. 5–7 also indicate that these raw images can provide reasonably close estimate of the void diameters. The results also show the ability to closely determine the relative location of a void in an extended SOFI panel. The

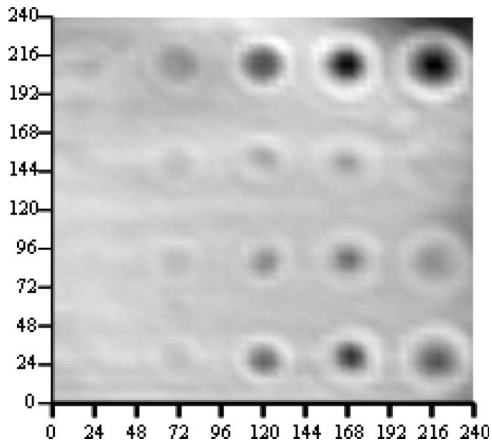


Fig. 7. SOFI panel #2 (70-GHz image) without adhesive between foam and aluminum substrate.

images shown thus far are the products of the combination of specific antenna radiation patterns and void geometries and dimensions. Therefore, it is possible to use deconvolution algorithms or other image enhancement techniques to remove the effect of antenna radiation pattern from these images, resulting in a closer size estimate and shape of a void [11], [12].

Figs. 8 and 9 show images of the 25- and 6-mm-diameter milled voids (i.e., flat-bottom-hole samples), respectively, in the single-slab, double-slab, and triple-slab sample combinations, using the 12-mm-diameter footprint lens antenna at 100 GHz. The results in Fig. 8 indicate that the voids with heights of (from left to right) 25, 18, 12, and 6 mm were detected at all three distance combinations above the substrate. The void with the smallest height of 3 mm can be seen on the single-slab and the triple-slab samples but not in the double-slab sample. One can also see from Fig. 9 that the 6-mm-diameter voids with heights (from left to right) of 25, 20, 10, and 5 mm were detected. However, clutter signal due to the small and nonuniform thickness gaps present in between different slabs resulted in masking out some of the voids. In practice, such artificial gaps do not exist, and therefore, this is not to be considered as a limitation when using this technique. Nevertheless, in this investigation, the presence of these gaps caused some masking of the desired signals from the voids.

It is important to note that lens antennas with smaller focusing footprints produce images that have higher spatial resolutions, which is the direct consequence of higher overall sensitivity to the presence of an anomaly. This fact is demonstrated by using the lens antenna with the smaller 6-mm-diameter footprint in conjunction with this sample set. Fig. 10 shows the image of the triple-slab case when the voids are located at the substrate using this lens. Comparison of this image with its counterpart using the previous lens [Fig. 8, triple slab (a)] shows that all five voids are clearly detected, whereas in Fig. 8, the smallest void is not very clearly detected.

It should be noted that the thicknesses of the triple-slab and the double-slab samples were comparable with focal lengths of the lenses used. Consequently, the images shown in Figs. 8 and 9 were obtained at distance between the lens antenna and the voids that was somewhat longer than focal length of the lens, which is 254 mm. Additionally, operating exactly at the focal lengths resulted in measurements that were sensitive to the presence of slight gaps that were mentioned earlier.

It is also important to further discuss the differences associated with the void images in Figs. 8 and 9. As shown in Fig. 8, although all the voids were milled with the same diameter, i.e., 25 mm, they do not project the same signature in the captured images. It is evident that as the height of the void decreases, its spatial signature appears to become fainter. This is mainly attributed to two factors. First, voids with larger volumes tend to have higher reflection than the ones with smaller volumes. Consequently, the small voids are more vulnerable to being masked out when in the vicinity of voids of higher volumes. Second, small voids are more susceptible to the presence of clutter (i.e., unwanted noise-like signal due to SOFI inhomogeneity, system noise, etc.). Consequently, by taking these two factors into account, the raw images (Figs. 8 and 9) can be enhanced considerably using simple image processing techniques such as that utilized below.

To enhance the captured images, it becomes crucial to estimate the clutter contaminating the raw data. Typically, this clutter appears as a low-pass signal with a dc component that possesses a gradient in one direction only, which is generally caused by standoff distance variation. Hence, it is sufficient to estimate this background dc component, which represents the clutter level, and subtract it from the raw data. To retrieve the signature of each void individually, the raw images were segmented, around a given void, after removing the clutter, resulting in each segment being normalized with respect to its local dynamic range. It is important to note that this procedure can be implemented without the need for *a priori* knowledge of the locations of the voids. This is especially true when the clutter level is relatively accurately estimated and removed, as described above. However, when the estimate of the clutter is biased, such as when the background signal is not very uniform, this technique may actually increase the clutter level in some cases. In this study, this situation may occur if there is significant level of material inhomogeneity associated with a region of the SOFI. Consequently, these regions may falsely indicate the presence of a void (i.e., false positive). To reduce the possibility of this from occurring, a threshold filtering followed by low-pass filtering is used after the segmented image is normalized with respect to its dynamic range. Basically, each intensity level in the normalized image is compared with a threshold value. Subsequently, all of the intensity levels that are below the threshold are filtered out, and the intensities that are greater than the threshold are preserved in the image. Fig. 11 shows the images of the 25-mm-diameter voids after applying the aforementioned technique with the threshold set at 0.35 (where a normalized image contains values from 0 to 1) followed by a $2 \times 2$ rectangular kernel as the low-pass filter. Comparing these images with their raw counterparts (Fig. 8, voids with a diameter of 25 mm), it is apparent that the processed images possess higher fidelity. In most cases, the spatial signatures of the voids can be readily retrieved from the processed images. Fig. 12 shows the results of this image enhancement technique when applied to the 6-mm-diameter voids. In this case, the threshold was set at 0.1, and a $2 \times 2$ rectangular kernel was used as a lowpass filter. Again, a comparison between these images and

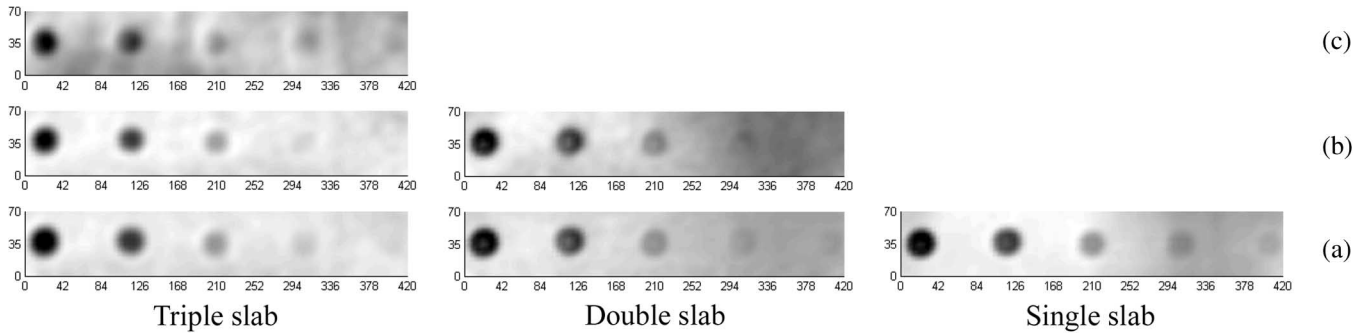


Fig. 8. One hundred-gigahertz images of 25-mm-diameter milled voids with different heights located in SOFI panels at different depths. (a) At substrate. (b) 70 mm from substrate. (c) 140 mm from substrate.

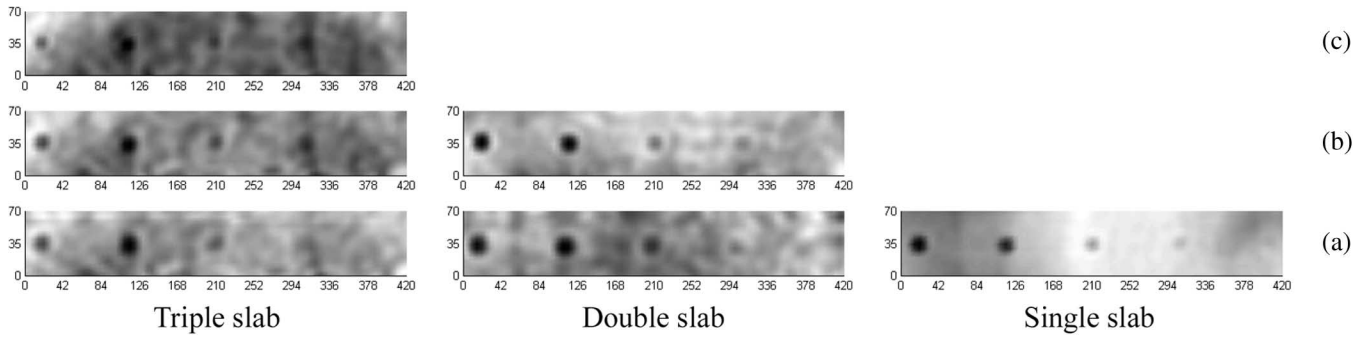


Fig. 9. One hundred-gigahertz images of 6-mm-diameter milled voids with different heights located in SOFI panels at different depths. (a) At substrate. (b) 70 mm from substrate. (c) 140 mm from substrate.

Fig. 10. One hundred-gigahertz images of 25-mm-diameter milled voids with different heights located in triple-slab SOFI panel at substrate obtained using the 6-mm-diameter footprint lens antenna.

those shown in Fig. 9 shows the resulting image enhancement, especially for the single-slab and the double-slab samples. In the former sample, however, this technique enhanced the clutter level as well as the desired signal. This is mainly due to the fact that the reflections from the nonuniformities, e.g., the slight and nonuniform gaps between the slabs, are comparable with those coming from the voids. As mentioned earlier, such an artificially introduced clutter is not expected to be encountered in practice. Thus, it is expected that this technique will perform well in real-life inspection scenarios.

The optimum threshold value can be set based on the desired probability of detection and the tolerable probability of false alarm (i.e., false positive). These probabilities are usually decided based on the reflected signal level, the clutter level, and the number of available realizations of the captured image. For instance, averaging several replicas of the image captured for the same anomalies (i.e., several voids) yields a higher probability of detection and a lower probability of false alarm. Intuitively, the optimum threshold level is different for different voids and imaging setups. Hence, one cannot assume a preset threshold level for all possible images. However, as a rule of thumb, a high threshold level is used when the minimum detectable void size is relatively large. On the other hand, when the system is designed to detect smaller voids, lower threshold levels that allow for weaker reflected signals to pass may be utilized.

## IV. Summary and Discussions

It is imperatively critical to detect and evaluate the properties of undesired manufactured or in-service produced anomalies such as voids and unbonds in the Space Shuttle's external tank SOFI. Millimeter-wave NDT methods have been shown to be viable candidates for life-cycle inspection of the SOFI. To this end, the primary objective of this investigation has been to assess the capabilities of these techniques for detecting localized anomalies as a function of their dimensions, location with SOFI thickness, and millimeter-wave inspection system properties. Several specifically manufactured SOFI panels were used in this investigation with embedded voids with varying diameters, heights, and locations within various SOFI panels. Millimeter-wave CW reflectometers at single frequencies of 33.5, 70, or 100 GHz representing a relatively wide range of millimeter-wave spectrum [Ka-band (26.5–40 GHz) to W-band (75–110 GHz)] were used to inspect these panels. Additionally, small horn and focused lens antennas were used in conjunction with these reflectometers, providing for the possibility of near-field and far-field measurements.

The overall results showed that small voids (diameter of 3 mm and height of 3 mm in 70-mm-thick SOFI and diameter of 6 mm and height of 2.5 mm in 140- and 210-mm-thick SOFI) were detected. It was also shown that these anomalies may be

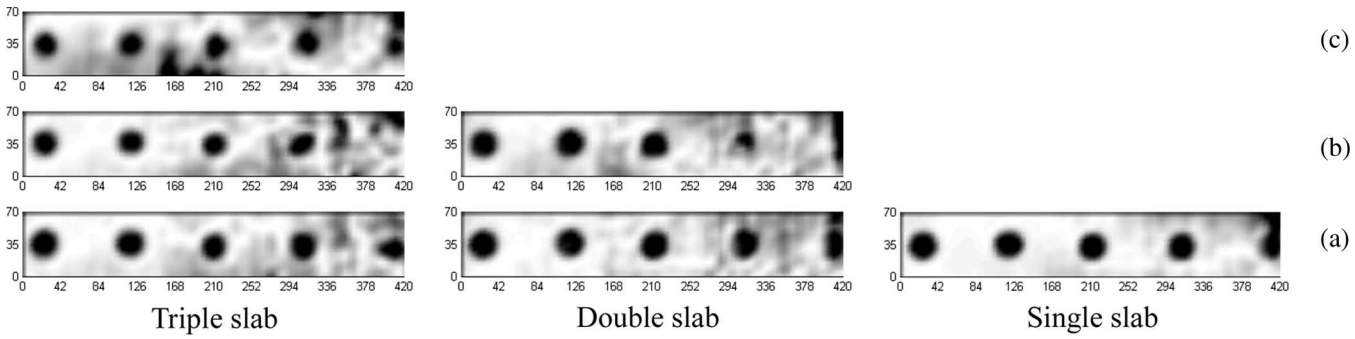


Fig. 11. Processed 100-GHz images of 25-mm-diameter milled voids with different heights located in SOFI panels at different depths. (a) At substrate. (b) 70 mm from substrate. (c) 140 mm from substrate.

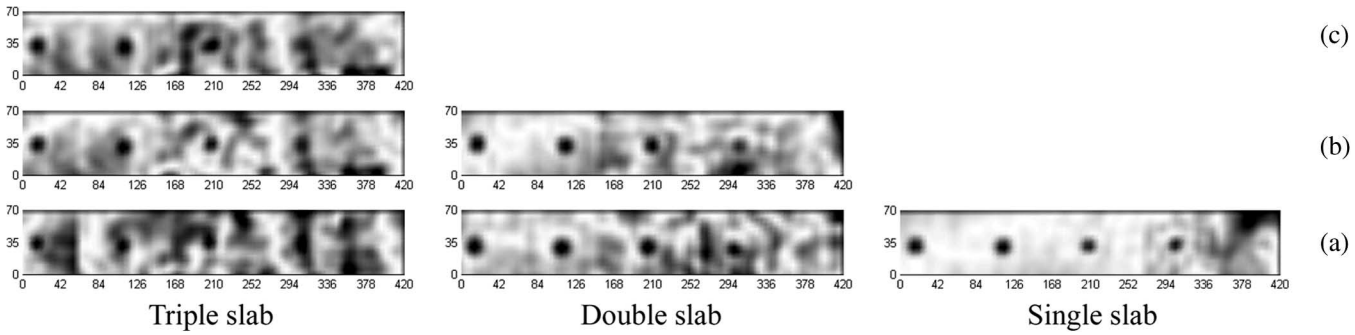


Fig. 12. Processed 100-GHz images of 6-mm-diameter milled voids with different heights located in SOFI panels at different depths. (a) At substrate. (b) 70 mm from substrate. (c) 140 mm from substrate.

detected in a relatively wide range of frequencies within the millimeter-wave frequency spectrum. It was also shown that frequency diversity may result in eliminating clutter sources such as the application of nonuniform adhesive. However, in these cases, this apparent gain was at a cost of reduction in spatial resolution (Fig. 5). In addition, the utility of small horn antennas as well as more sophisticated focused lens antennas was also demonstrated. Operating in the near-field region of a horn antenna produced informative (both quantitative and qualitative) images. As expected, high-resolution images were produced using the focused lens antennas. Small horn antennas seemed to provide better detection of anomalies in a relatively thin SOFI, whereas the focused lens antennas performed much better when inspecting a relatively thick SOFI.

Several panels used in this investigation had thicknesses that were comparable with the focal lengths of the lenses used. Consequently, in these cases, the distance between the lens antennas and the voids was somewhat longer than the focal lengths. Nevertheless, small voids right above the substrates as well as small voids at different depths within the SOFI slabs were detected. This is an advantage of using these techniques because multiple voids located at different depths within the SOFI can be simultaneously detected in one scan/image (i.e., no need to change lens distance to a panel to detect voids at different depths). This fact has also been demonstrated in a previous investigation [7]. It should be noted that the utility of small horn antennas provides for detecting multiple voids located at different depths within relatively thin SOFI similar to the lens antenna.

The lens with the smaller footprint produced higher spatial resolution images. One must be careful that, in this case, the small footprint associated with the lens may also contribute to a higher level of clutter produced as a result of small nonuniformities with SOFI. To this end, a relatively simple image processing algorithm was successfully implemented to obtain more information about the properties of the embedded voids.

## REFERENCES

[1] "Columbia accident investigation board report," NASA, Aug. 2003.
[2] E. Generazio, "The national aeronautics and space administration nondestructive evaluation program for safe and reliable operations," in *Proc. 32nd Annu. Rev. Progress in Quantitative Nondestructive Evaluation*, D. O. Thompson and D. E. Chimenti, Eds. Melville, NY: Amer. Inst. Phys., 2005, vol. 25A, pp. 2–21.
[3] R. Zoughi, S. Kharkovsky, and F. Hepburn, "Microwave and millimeter wave testing for the inspection of the space shuttle spray on foam insulation (SOFI) and the acreage heat tiles," in *Proc. 32nd Annu. Rev. Progress in Quantitative Nondestructive Evaluation*, D. O. Thompson and D. E. Chimenti, Eds. Melville, NY: Amer. Inst. Phys., 2005, vol. 25A, pp. 439–446.
[4] C. P. Chiou, R. B. Thompson, W. P. Winfree, E. I. Madaras, and J. Seebo, "Modelling and processing of terahertz imaging in space shuttle external tank foam inspection," in *Proc. 32nd Annu. Rev. Progress in Quantitative Nondestructive Evaluation*, D. O. Thompson and D. E. Chimenti, Eds. Melville, NY: Amer. Inst. Phys., 2005, vol. 25A, pp. 484–491.
[5] S. Shrestha, S. Kharkovsky, R. Zoughi, and F. L. Hepburn, "Microwave and millimeter wave nondestructive evaluation of the external tank insulating foam," *Mater. Eval.*, vol. 63, no. 3, pp. 339–344, Mar. 2005.
[6] S. Kharkovsky, F. Hepburn, J. Walker, and R. Zoughi, "Nondestructive testing of the space shuttle external tank foam insulation using near field and focused millimeter wave techniques," *Mater. Eval.*, vol. 63, no. 5, pp. 516–522, May 2005.

[7] S. Kharkovsky, J. T. Case, R. Zoughi, and F. Hepburn, "Millimeter wave detection of localized anomalies in the space shuttle external fuel tank insulating foam and acreage heat tiles," in *Proc. 22nd IEEE Instrum. and Meas. Technol. Conf.*, Ottawa, ON, Canada, 2005, pp. 1527–1530.
[8] R. Zoughi, *Microwave Non-Destructive Testing and Evaluation*. Dordrecht, The Netherlands: Kluwer, 2000.
[9] S. Bakhtiari, S. Ganchev, N. Qaddoumi, and R. Zoughi, "Microwave non-contact examination of disbond and thickness variation in stratified composite media," *IEEE Trans. Microw. Theory Tech.*, vol. 42, no. 3, pp. 389–395, Mar. 1994.
[10] C. A. Balanis, *Antenna Theory: Analysis and Design*, 2nd ed. New York: Wiley, 1997.
[11] A. K. Nandi and D. Mampel, "Deconvolution of ultrasonic signals in nondestructive testing applications," in *Proc. IEEE Signal Process./ATHOS Workshop Higher-Statistics*, Girona, Spain, Jun. 1995, pp. 243–247.
[12] G. Hayward and J. E. Lewis, "Comparison of some non-adaptive deconvolution techniques for resolution enhancement of ultrasonic data," *Ultrasonics*, vol. 27, no. 5, pp. 155–164, May 1977.

**Sergey Kharkovsky** (M'00–SM'03) received the degree in electronics engineering from Kharkov Institute of Radioelectronics, Kharkov, Ukraine, in 1975, the Ph.D. degree in radiophysics from Kharkov State University, Kharkov, in 1985, and the D.Sc. degree in radiophysics from the Institute of Radio-Physics and Electronics (IRE), National Academy of Sciences of Ukraine, Kharkov, in 1994.

Currently, he is a Research Associate Professor with the Department of Electrical and Computer Engineering, University of Missouri–Rolla (UMR), Rolla, MO. Prior to joining UMR, he was a Member of the Research Staff at IRE from 1975 to 1998 and a Professor in the Department of Electrical and Electronics Engineering, Cukurova University, Adana, Turkey, from 1998 to 2002. He was a Visiting Associate Professor in the Department of Electrical and Computer Engineering, UMR, from March 2003 to February 2006. His research area with IRE was the investigation and development of new millimeter-wave techniques including dielectric resonators with whispering gallery modes, solid-state oscillators, and their application for material characterization. His current research interest is nondestructive testing and evaluation of composite structures using microwaves and millimeter waves.

**Joseph T. Case** (S'99) received the dual B.S. degree in electrical engineering and physics and the M.S. degree from the University of Missouri–Rolla (UMR), Rolla, MO, in 2003 and May 2006, respectively, after also attending both Northern Arizona University, Flagstaff, and Colorado State University, Fort Collins. He is currently working toward the Ph.D. degree in electrical engineering at UMR, with an emphasis in microwave nondestructive evaluation (NDE).

Since 1999, he has been with the Applied Microwave Nondestructive Testing Laboratory, UMR, as an Undergraduate Research Assistant and Graduate Research Assistant. His current research interests include applying synthetic aperture focusing and holographical methods to microwave NDE.

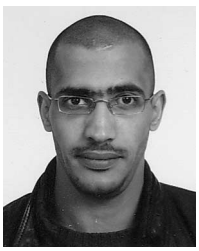

**Mohamed A. Abou-Khousa** (S'01) received the B.S.E.E. degree (*magna cum laude*) from the American University of Sharjah, Sharjah, United Arab Emirates, in 2003 and the M.S.E.E. degree from Concordia University, Montreal, QC, Canada, in 2004. He is currently working toward the Ph.D. degree at the University of Missouri–Rolla (UMR), Rolla, MO.

Since January 2005, he has been with the Applied Microwave Nondestructive Testing Laboratory, UMR, as a Graduate Research Assistant. His research interests include millimeter-wave and microwave nondestructive testing, synchronization in spread spectrum systems, and high-resolution spectral estimation techniques.

**Reza Zoughi** (S'86–M'87–SM'93–F'06) received the B.S.E.E., M.S.E.E., and Ph.D. degrees from the University of Kansas, Manhattan, all in electrical engineering (radar remote sensing, radar systems, and microwaves).

From 1981 to 1987, he was with the Radar Systems and Remote Sensing Laboratory, University of Kansas. Currently, he is the Schlumberger Distinguished Professor of electrical and computer engineering at the University of Missouri–Rolla (UMR), Rolla, MO. Prior to joining UMR in January 2001 and since 1987, he was with the Department of Electrical and Computer Engineering, Colorado State University (CSU), Fort Collins, where he was a Professor and established the Applied Microwave Nondestructive Testing Laboratory. He held the position of Business Challenge Endowed Professor of electrical and computer engineering from 1995 to 1997 while at CSU. He has to his credit more than 350 journal publications, conference proceedings and presentations, technical reports, and overview articles. He is the author of a graduate textbook entitled *Microwave Nondestructive Testing and Evaluation Principles* (Boston, MA: Kluwer, 2000) and the coauthor of a chapter on "Microwave Techniques" in an undergraduate introductory textbook entitled *Nondestructive Evaluation: Theory, Techniques, and Applications* (New York: Marcel Dekker, 2002). He holds seven patents all in the field of microwave nondestructive testing and evaluation. His current areas of research include developing new nondestructive techniques for microwave- and millimeter-wave inspection and testing of materials (NDT), developing new electromagnetic probes to measure characteristic properties of material at microwave frequencies, and developing embedded modulated scattering techniques for NDT purposes, in particular for complex composite structures.

Dr. Zoughi is a Fellow of the American Society for Nondestructive Testing (ASNT). He is the Associate Editor-in-Chief for the IEEE TRANSACTIONS ON INSTRUMENTATION AND MEASUREMENT, Editor for *Research in Nondestructive Evaluation*, and Technical Associate Editor for *Materials Evaluation*. He served as the Guest Associate Editor for the Special Microwave NDE Issue of *Research in Nondestructive Evaluation* in 1995 and Co-Guest Editor for the Special Issue of *Subsurface Sensing Technologies and Applications: Advances and Applications in Microwave and Millimeter Wave Nondestructive Evaluation*. He served as the Research Symposium Co-Chair for the ASNT Spring Conference and 11th Annual Research Symposium in March 2002 in Portland, OR, and as the Technical Chair for the IEEE Instrumentation and Measurement Technology Conference (IMTC2003) in May 2003 in Vail, CO. He served as the Guest Editor for the IMTC2003 special issue of the IEEE TRANSACTIONS ON INSTRUMENTATION AND MEASUREMENT. In the past five years at UMR, he has received two Outstanding Teaching Commendations, two Outstanding Teaching Awards, and two Dean of Engineering Excellence in Teaching Awards. He was voted the Most Outstanding Teaching Faculty seven times by the junior and senior students at the Department of Electrical and Computer Engineering, CSU. He received the College of Engineering Abell Faculty Teaching Award in 1995. He is the 1996 recipient of the Colorado State Board of Agriculture Excellence in Undergraduate Teaching Award (only one faculty recognized for this award at each of the three CSU system campuses). He was recognized as an honored researcher for seven years by the Colorado State University Research Foundation. He is also a member of Sigma Xi and Eta Kappa Nu.

**Frank L. Hepburn** received the B.S. degree in electrical engineering from California Polytechnic State University, San Luis Obispo, in 1982.

He was an Engineer for Piper Aircraft (Santa Maria, CA, and Vero Beach, FL) from 1980 to 1982, for United Space Boosters, Inc. (Vandenberg Air Force Base) from 1982 to 1984, for Lockheed Space Operation (SPC Contract with NASA and Air Force Vandenberg Air Force Base) from 1984 to 1987, and for Boeing Aerospace Operations (Marshall Space Flight Center) from 1987 to 1988. He has been an Engineer with NASA Marshall Space Flight Center, AL, since 1988, where he initiated and implemented the first Nondestructive Evaluation Microwave and Millimeter Wave Laboratory within NASA.